

Real-time digital holographic beam-shaping system with a genetic feedback tuning loop

Joonku Hahn, Hwi Kim, Kyongsik Choi, and Byoung-ho Lee

A novel implementation of a real-time digital holographic system with a genetic feedback tuning loop is proposed. The proposed genetic feedback tuning loop is effective in encoding optimal phase holograms on a liquid-crystal spatial light modulator in the system. Optimal calibration of the liquid-crystal spatial light modulator can be achieved via the genetic feedback tuning loop, and the optimal phase hologram can then overcome the aberration of the internal optics of the system. © 2006 Optical Society of America

OCIS codes: 050.1970, 070.4560, 090.1000, 090.1970.

1. Introduction

In digital holography, designing phase holograms that produce the desired diffraction images is one of the most important engineering goals. The design and fabrication of phase holograms or holographic (diffractive) optical elements have been intensively investigated over the past two decades.^{1–3} Real-time dynamic digital holography using a liquid-crystal spatial light modulator (LCSLM) has recently become more attractive than surface-relief fixed-type holographic (diffractive) optical elements. Real-time dynamic digital holographic beam-shaping technologies are useful in a wide range of applications, including telecommunications, displays, optical storage, and optical information processing, and they are currently being extensively studied.^{4–6}

In general, the design and implementation of a digital holographic beam-shaping system is as follows. Continuous phase holograms are designed with the aid of design algorithms such as the iterative Fourier-transform algorithm (IFTA).^{7,8} The quantized phase hologram is next encoded on the LCSLM. An incident beam on the LCSLM is diffracted (transformed) through the internal optics of the beam-shaping system and generates images in the image plane. Modulating the phase of the incident beam so as to have the designed value for each pixel of the LCSLM is important for achieving effi-

cient and accurate beam shaping.⁹ In the phase-hologram design stage, the ideal mathematical model for an optical system is assumed. In general, the internal optical system of the beam-shaping system is mathematically modeled based on the linear canonical transform (LCT).⁸ However, in practical systems, several physical factors, such as phase- and amplitude-modulation errors induced in each cell of the LCSLM, misalignment of the optical components, and aberrations, may induce a difference between ideal simulation results and experimental results obtained in a real system. In terms of implementing a practical system, analysis of the errors caused by these physical factors and relevant fine-tuning are important for obtaining optimal diffraction images. In general, this fine-tuning is perceived as somewhat intricate since the origins of the errors are various, the theoretical identification of the errors for optimal compensation is not easy, and the optimization of many system parameters requires a novel system and may complicate the final configuration of the system. In addition, the fine-tuning problem cannot be addressed at the design stage but is applied at the system-implementation stage. The fine-tuning technique should be robust, reliable, and reproducible.

In this paper the novel implementation of a real-time digital holographic beam-shaping system with a LCSLM, having a specially devised fine-tuning process referred to as the genetic feedback tuning loop, is proposed. The genetic feedback tuning loop is based on a well-known genetic algorithm.^{7,10} The results show that the proposed genetic feedback tuning loop is effective in encoding optimal phase holograms for overcoming several physical factors that degrade the performance of a practical system.

The authors are with the School of Electrical Engineering, Seoul National University, Kwanak-Gu Shinlim-Dong, Seoul 151-744, South Korea. B. Lee's e-mail address is byoung-ho@snu.ac.kr.

Received 11 May 2005; accepted 12 July 2005.

0003-6935/06/050915-10\$15.00/0

© 2006 Optical Society of America

This paper is organized as follows. In Section 2 the causes of the degradation of diffraction images in practical digital holographic beam-shaping systems are discussed. The objects to be treated for optimally tuning the system are identified and formulated. In Section 3 the proposed genetic fine-tuning loop is described. In Section 4 the real-time holographic beam-shaping system with the genetic feedback tuning loop is experimentally realized. In Section 5 concluding remarks and perspectives for the devised system are provided.

2. Causes Degrading Diffraction Images in Practical Digital Holographic Beam-Shaping Systems

In this section the causes behind the degradation of diffraction images in a practical digital holographic beam-shaping system with a LCSLM are identified and analyzed. Figure 1 shows a schematic diagram of a practical LCSLM holographic beam-shaping system, which consists of a laser, a beam expander, a LCSLM, two polarizers, and a Fourier lens with focal length f . The phase-modulation range (including the maximum phase modulation of the 2π phase shift) can be realized in the LCSLM by using appropriate polarizers. The incident optical wave impinges on the back side of the LCSLM and then passes through the LCSLM with its phase modified. The modulated optical wave is transformed by the optical system to form a diffraction image in the image plane. In this configuration the two main causes for the degradation of the diffraction image are incorrect SLM calibration and aberrations present in the internal optics of the beam-shaping system. Accordingly, in this paper we focus on the appropriate treatment for SLM calibration and the aberration compensation of the beam-shaping system.

First, we discuss SLM calibration. In the design stage a continuous phase hologram is obtained by the IFTA. In practice, the possible phase-modulation levels at the pixels of the SLM are quantized, and the relationship between the phase-modulation level and the quantization number is typically nonlinear, which is referred to as the phase-modulation table of the SLM. The SLM with 8 bit resolution controls the phase-modulation level at each pixel by an integer called the encoding index, which ranges from 0 to 255. The SLM should be calibrated by finding the relationship between the phase-modulation level and the encoding index, i.e., a phase-modulation table. In addition, accurate characterization of the transmittance of the phase-modulation devices is important in the field of diffractive optics. The nonlinear transmittance model should be taken into account for fabricated diffractive optical elements as well as for the LCSLM.¹¹ Although the accurate modeling of the transmittance of a practical SLM is more complicated,^{12–15} the phase-modulation characteristics of the SLM can be easily characterized by using experimental approaches. The first procedure of tuning is finding

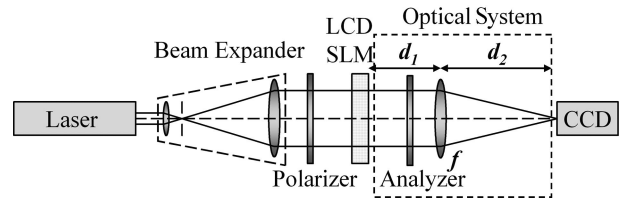


Fig. 1. Schematic of the digital holographic beam-shaping system.

the nonlinear phase-modulation table. This type of calibration is typically accomplished by interferometric methods. However, in our system the calibration is considered to be an optimization problem. It will be shown that this approach is also effective for SLM calibration. For the optimization scheme, the cost function to be maximized and unknown variables to be optimized need to be identified. In this case of the SLM with 256 encoding indices, the number of unknown variables is 254, since the first level and the last level are fixed as the phase modulation of 0 and 2π , respectively. The phase-modulation level of a pixel on the SLM is controlled by a signal designed with an integer number. When the phase modulation for an input integer n is denoted by p_n , the phase-modulation levels p_n s are the unknown variables to be found. In this paper we assume a monotonic relationship between the input integer and the phase-modulation level. Hence the cost function F is parameterized by 254 unknown variables p_n and the optimization problem is defined as

$$\begin{aligned} \max F[p_1, p_2, p_3, \dots, p_{254}] \\ \text{for } 0 \leq p_1 \leq p_2 \leq \dots \leq p_{254} \leq 2\pi, \end{aligned} \quad (1)$$

the definition of which is completely described in Section 3.

We next discuss the aberration of the beam-shaping system and its compensation. Let the distance from the hologram plane to the lens and that from the lens to the image plane be d_1 and d_2 , respectively, as shown in Fig. 1. Let the wavelength of the optical wave be λ . The transform of the optical system $\text{Fr}[\]$ is represented as the LCT or the generalized Fresnel transform⁸

$$\begin{aligned} F(x_2, y_2) &= \text{Fr}[G(x_1, y_1)] \\ &= \int_{-\infty}^{\infty} \int_{-\infty}^{\infty} h(x_2, y_2, x_1, y_1) G(x_1, y_1) dx_1 dy_1, \end{aligned} \quad (2)$$

where (x_1, y_1) and (x_2, y_2) denote the coordinates of a point in the SLM plane and that in the image plane, respectively, and $h(x_2, y_2, x_1, y_1)$ is the propagator of the Fresnel transform and takes the form

$$\begin{aligned}
h(x_2, y_2, x_1, y_1) = & \frac{-j}{\left| \lambda(d_1 + d_2) - \frac{\lambda d_1 d_2}{f} \right|} \\
& \times \exp \left\{ \frac{j\pi}{\lambda(d_1 + d_2) - \frac{\lambda d_1 d_2}{f}} \right. \\
& \times \left[\left(1 - \frac{d_1}{f} \right) (x_2^2 + y_2^2) - 2(x_2 x_1 \right. \\
& \left. + y_2 y_1) + \left(1 - \frac{d_2}{f} \right) (x_1^2 + y_1^2) \right] \left. \right\}. \quad (3)
\end{aligned}$$

The optical field that just passed through the SLM with a phase hologram encoded is denoted by $G(x_1, y_1)$. In the phase-only modulation mode of the SLM, $G(x_1, y_1)$ is represented as

$$G(x_1, y_1) = A \exp[j\Phi(x_1, y_1)], \quad (4)$$

where $\Phi(x_1, y_1)$ is the phase hologram encoded on the SLM and A indicates a constant amplitude. In an aberration-free situation, the phase hologram designed by the IFTA may be directly used as the final phase hologram to be encoded on the SLM. However, defocusing, misalignment of the optical elements, and aberrations cause the real transform to deviate from the ideal model of Eq. (3). These factors are system dependent.

The aberration can be theoretically analyzed based on diffraction theory.¹⁶ The most general representation of the aberration is based on Zernike polynomials. Let the aberration of the optical system be represented by $\Omega(x_1, y_1)$ and the mathematical expression of the transform of the real system read as

$$h_{\text{real}}(x_2, y_2, x_1, y_1) = h(x_2, y_2, x_1, y_1) \exp[j\Omega(x_1, y_1)]. \quad (5)$$

The compensated optical field $G'(x_1, y_1)$ should take the following form:

$$G'(x_1, y_1) = A \exp[j\Phi(x_1, y_1)] \exp[-j\Omega(x_1, y_1)]. \quad (6)$$

The addition of a conjugate phase term $\exp[-j\Omega(x_1, y_1)]$ for system aberration to the designed phase hologram will compensate for the distortion of the diffraction image induced by the aberration. The aberration component of the optical system $\Omega(x_1, y_1)$ is given by the weighted sum of Zernike polynomials as

$$\begin{aligned}
\Omega(x_1, y_1) = & \Omega(\rho, \theta) \\
= & A_{00} + \frac{1}{\sqrt{2}} \sum_{n=2}^{\infty} A_{n0} R_n^0(\rho) + \sum_{n=1}^{\infty} \sum_{m=1}^n A_{nm} R_n^m(\rho) \\
& \times \cos m\theta + \sum_{n=1}^{\infty} \sum_{m=1}^n A_{nm}' R_n^m(\rho) \sin m\theta, \quad (7)
\end{aligned}$$

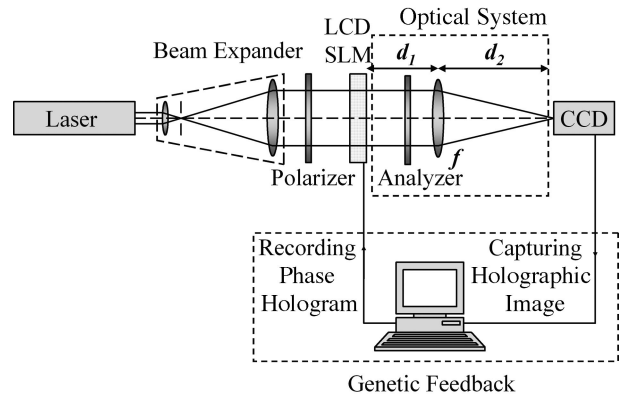


Fig. 2. Schematic of a real-time digital holographic beam-shaping system with a genetic feedback tuning loop.

where A_{nm} and A_{nm}' denote the coefficients of terms having an x -axis symmetry and a y -axis symmetry, respectively, and $R_n^m(\rho)$ denotes the circular Zernike polynomial of the order (m, n) . And ρ and θ are, respectively, given by

$$\rho = [(x - x_c)^2 + (y - y_c)^2]^{1/2}, \quad (8)$$

$$\theta = \tan^{-1} \left(\frac{y - y_c}{x - x_c} \right), \quad (9)$$

where (x_c, y_c) indicates the center of the Zernike polynomials. The second procedure for tuning is compensating for the internal aberration of the optics of the beam-shaping system. In this case the unknown variables to be optimized are coefficients and the center position of the Zernike polynomials. The cost function F is then parameterized by the coefficients of the Zernike polynomials and the center position. The optimization problem is expressed as

$$\max F[A_{nm}, A_{nm}', x_c, y_c].$$

The truncation order of the Zernike polynomial is determined by considering the sampling resolution of the SLM and the computation cost.

In this paper a powerful and general optimization technique, a genetic algorithm, is applied to find the nonlinear phase-modulation table of the SLM and the aberration-compensated phase holograms to be encoded on the SLM of the beam-shaping system. Since the inverse transform of the real optical system from the CCD plane to the SLM domain does not exist, an efficient and effective genetic optimization algorithm that uses only the forward transform from the SLM domain to the CCD plane is employed. The proposed fine-tuning technique of the digital holographic beam-shaping system evaluates the qualities of the diffraction images on the CCD plane and feeds this information back to the holograms on the SLM domain with the genetic algorithm. The genetic algorithm enables all system parameters, i.e., nonlinear phase-modulation table and coefficients of Zernike

polynomials for aberration compensation, to be automatically fine-tuned.

In the following sections, detailed methods related to the two procedures of tuning are described. The experimental implementation of the real-time digital holographic beam-shaping system with the genetic feedback tuning loop is developed and the feasibility of finely tuning the beam-shaping system and finding the optimal phase holograms is described. The nonlinear phase-modulation table of the SLM is extracted and applied to the SLM to obtain an enhanced diffraction image. The aberration of the internal optics of the diffractive beam-shaping system is compensated by improving the phase hologram through the genetic feedback tuning loop. The resulting improved diffractive images generated by the tuned beam-shaping system are presented.

3. Genetic Feedback Tuning Loop

In this section the proposed genetic feedback tuning loop for fine-tuning the real system is described. Figure 2 shows a schematic diagram of the devised system with the genetic feedback tuning loop. As shown in Fig. 2, the feedback loop is constructed between the CCD and the SLM through a computer. The CCD captures the energy distribution of the diffracted field at the image plane. The captured image is transported to a computer for evaluating the quality of the diffraction image, which is part of the genetic optimization of the system parameters identified in Section 2. The system parameters modified by the computer are sent to the SLM, which then modifies the diffraction image captured by the CCD. The evaluation process in the computer is repeated. The genetic algorithm implemented in the computer gradually enhances the diffraction image by tuning the system parameters. This iterative feedback loop is referred to as the genetic feedback tuning loop.

In general, the genetic algorithm searches local optima through two distinguished operations, crossover and mutation. Conceptually, the crossover operation is effective in convex optimization problems, since the crossover operation is mathematically analogous to the linear combination of two chromosomes in a floating-point coding scheme. The mutation is simply a random search, making the small variations in the present solution. If the present solution is not a local optimum, small variations will lead to an improvement in the present solution. The mutation operation is more general in the genetic algorithm.

In our system two factors, i.e., the nonlinear phase-modulation relationship of the SLM and the dynamic aberration compensation, are focused on. It is ambiguous that the crossover operation is effective, since the related optimization problem may not be convex. Thus, for convenience and low computation cost, only the mutation operation is employed in our application. Hence a somewhat simplified genetic algorithm scheme is devised for use in our system.

Figure 3 shows a flow chart of the simplified genetic algorithm implemented in the genetic feedback tuning loop shown in Fig. 2. It should be noted that the

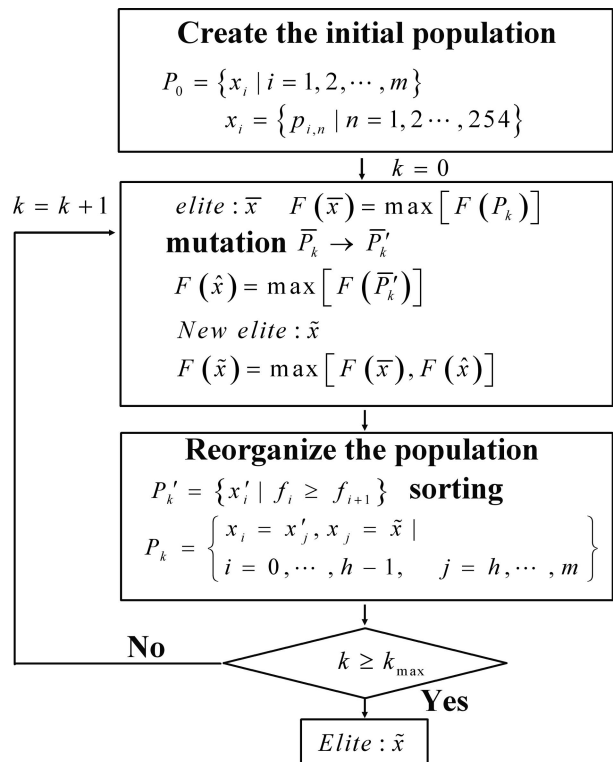


Fig. 3. Flow chart for the simplified genetic algorithm implemented in the genetic feedback tuning loop.

expression in the flow chart corresponds to the case of finding the phase-modulation table of the SLM. First, the initial population P_0 of a population size m is selected. The population is composed of subset x_i , which has 254 elements in accordance with the encoding indices. The unknown variable $P_{i,n}$, that is, the element of x_i , means the relative phase delay of the $(n + 1)$ th encoding index. The cost values $F(P_0)$ of chromosomes in the initial population are next calculated, and, the fittest chromosome with the largest cost value, i.e., the elite \bar{x} , is determined [see problem (1)]. The cost function F is the weighted linear combination of the standard evaluation factors of the obtained diffraction image, the definition of which is completely described in Section 4. The mutation operation is next applied to the initial population P_0 , and the modified population \bar{P}'_0 is then obtained. For the mutation, an adaptive mutation operator for floating-point coding is implemented, in which the mutation probability and the system parameter for determining the degree of nonuniformity are tuned to ~ 0.03 and 20 (see Chaps. 5 and 6 of Ref. 10). The system parameter, which indicates the degree of nonuniformity, effectively controls the convergence speed of the genetic algorithm. It should be noted that the evaluation of each chromosome requires a complete signal flow along the path of encoding the phase hologram on the SLM, capturing the resulting diffraction image by the CCD, and evaluating the cost value of the chromosome. Thus, to achieve one generation of the genetic algorithm, several sequential repetitions of encoding and capturing should be made.

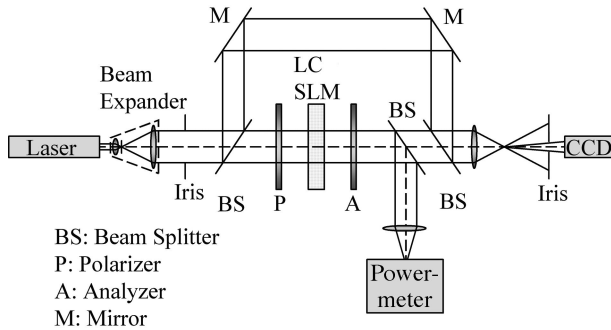


Fig. 4. Schematic of the interferometer for measuring the phase modulation and amplitude transmission of the LC SLM

In the case of compensating for the internal aberration of the optics of the beam-shaping system, the coefficients of the Zernike polynomials A_{nm} , A_{nm}' and the center position (x_c, y_c) are substituted into $P_{i,n}$ in the flow chart shown in Fig. 3. Consequently, the number of the unknown variables is also changed.

4. Experimental Realization of a Digital Holographic Beam-Shaping System with a Genetic Feedback Tuning Loop

In this section an experimental realization of the digital holographic beam-shaping system with the genetic feedback tuning loop is presented and some experimental results are shown. In Subsection 4.A the structure of the cost function for evaluating the obtained diffraction images is devised. In Subsection 4.B the phase modulation and amplitude transmission characteristics of the SLM used are inspected by means of an interferometric experiment, and these data are compared with data obtained using the genetic feedback loop. In Subsection 4.C the experimental evidence of the aberration compensation attained by the proposed method is given.

A. Cost Function for Evaluating Diffraction Images

In this paper the desired diffraction image to be generated in the image plane, namely, the target image, is a simple, conventional binary image, the bright region of which is termed the signal region and the region outside the signal region is called the noise region. The binary target image is used to evaluate real diffraction images that have continu-

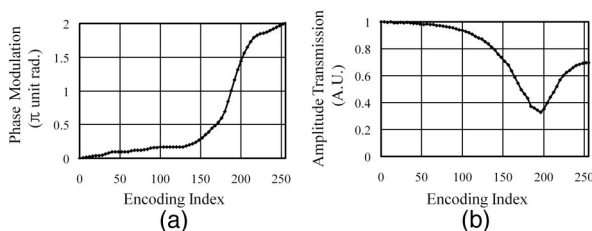


Fig. 5. Characteristics of the LC SLM measured by interferometric methods: (a) phase modulation versus encoding index and (b) amplitude transmission versus encoding index.

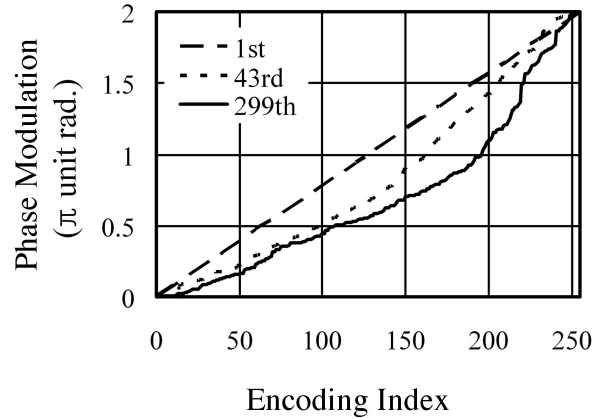


Fig. 6. Comparison of the phase-modulation tables obtained at three different stages of generation (1st, 43rd, and 299th) in SLM calibration.

ous brightness. The brightness of diffraction images captured by the CCD with an 8 bit resolution is quantized into 256, and this quantized brightness level is referred to as a gray level.

The cost function is devised to minimize the deviation of a diffraction image from the target image and the length of the boundary, which is the number of edge pixels across the threshold in a diffraction image. We evaluate a diffraction image in a local process in which the partial cost of each pixel contributes linearly to the cost of a diffraction image. This process requires a low computation cost and is effective in tuning our system with the genetic feedback tuning loop.

The deviation of a diffraction image is separated into the intensity of deviation from the target image in the signal region and the variation in intensity in the noise region. Minimizing the cost function must increase the transmission efficiency (brightness) in the signal area and decrease the mean-square error between the target image and the diffraction image. Let the gray level at position (x_2, y_2) in the real diffraction image captured by the CCD be denoted by $GL(x_2, y_2)$, then the normalized mean-square error in the signal region is defined as

$$\text{Mean-square error} = \frac{\sum_s \left[\frac{GL(x_2, y_2) - 255}{255} \right]^2}{\sum_s 1}, \quad (10)$$

where \sum_s denotes the summation in the signal region and the denominator $\sum_s 1$ indicates the area of the signal region. In experiments some bright spots often appear in a captured image and it is impossible to reduce the average of the gray levels in the noise region to zero. These bright spots increase the statistical variation value of the intensity distribution in the noise region. The variation in the image reflects the quality of the image better than the deviation from zero in the noise region. The normalized variation in the noise region is defined as

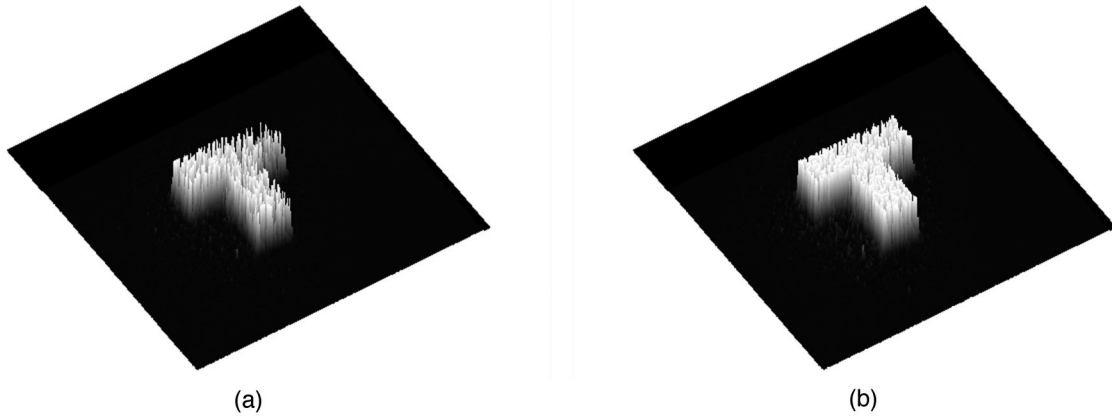


Fig. 7. Diffraction images observed during the calibration of the SLM with the genetic feedback tuning loop at (a) the 1st generation stage and (b) the 299th generation stage (the stagnated state).

$$\text{Normalized variation} = \frac{\sum_N \left[\frac{\text{GL}(x_2, y_2) - \overline{\text{GL}_N}}{\overline{\text{GL}_N}} \right]^2}{\sum_N 1}, \quad (11)$$

$$\overline{\text{GL}_N} = \frac{\sum_N \text{GL}(x_2, y_2)}{\sum_N 1}, \quad (12)$$

where \sum_N denotes the summation in the noise region and $\overline{\text{GL}_N}$ indicates the average of the gray levels in the noise region. A decrease in the normalized vari-

of the system. Since the internal aberration deforms a diffraction image, the boundary length increases generally. Therefore, in practice, the boundary length decreases as the aberration is compensated. On the other hand, the boundary length is stationary as the phase-modulation table of the SLM changes. Therefore the boundary length must be considered to evaluate the quality of the image only when the system is tuned for aberration compensation. The boundary length is defined as

$$\text{Boundary length} = \sum_{S+N} \text{edge}(x_2, y_2), \quad (13)$$

$$\text{edge}(x_2, y_2) = \begin{cases} 1 & \text{if } \text{GL}(x_2, y_2) > \text{threshold and } \text{GL}(x_2', y_2') < \text{threshold} \\ 0 & \text{otherwise} \end{cases}, \quad (14)$$

ation will restrain the appearance of bright spots in the noise region of a diffraction image. On the other hand, there is an intricate problem associated with the experiment. The measured system is sensitive to external noise, such as vibration, fluctuations in the light source, and scattering. However, a stable system is essential to the operation of the genetic feedback loop. Therefore, to achieve stability, the deviation value is compensated by a stabilization factor so that the deviation in the diffraction image with the same phase hologram and system parameters remains constant with time. For this, we use the initially selected reference phase hologram and its deviation of a diffraction image as the reference value. In practice, the reference phase hologram does not produce the same deviation value, and a stabilization factor is defined as the ratio of a temporal deviation value to the reference value. We obtain a stabilization factor in every generation and correct the deviation value by multiplying by a stabilization factor.

The boundary length in a diffraction image changes extensively when the hologram on the SLM is modified to compensate for the aberration of the internal optics

where (x_2', y_2') is the point adjacent to (x_2, y_2) in a diffraction image captured by the CCD and the threshold is a fixed value (60 in our system).

The cost function for evaluating the diffraction image is given by the weighted sum of the three evaluation Eqs. (10), (11), and (13). The appropriate weights are necessary for the correct and stable convergence of the genetic algorithm and are selected from experience. In our system we set the weight of the normalized variation as -1 , the mean-square er-

Table 1. Evaluation Parameters of Diffraction Images in Spatial Light Modulator Calibration

Generation	1st Generation	299th Generation
$\overline{\text{GL}_S}^a$	114.1	158.5
$\overline{\text{GL}_N}$	10.7	11.4
Mean-square error	0.3806	0.2408
Normalized variation	0.5742	1.198
Stabilization factor	0.9896	1.006
Cost value	-38.23	-25.41

^a $\overline{\text{GL}_S}$ denotes the average of the gray levels in the signal region.

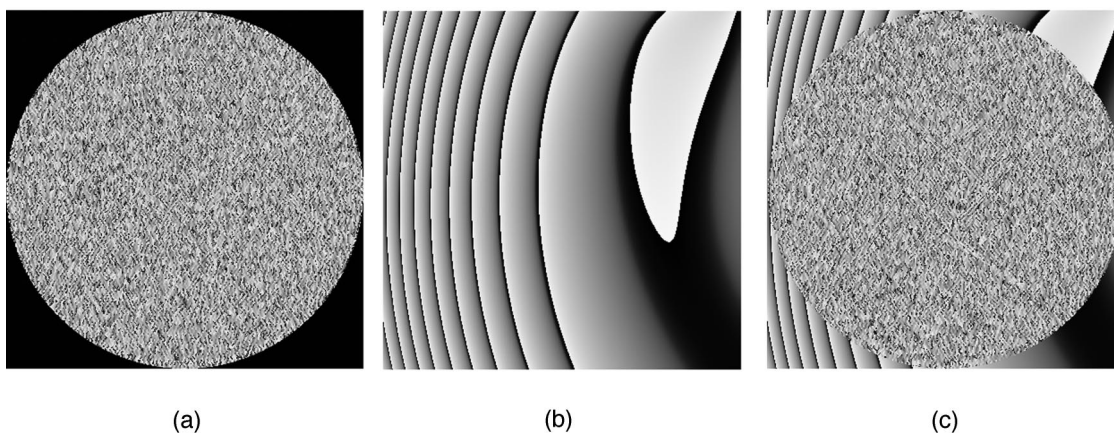


Fig. 8. Phase holograms and aberration compensation: (a) phase holograms without compensation at the 1st generation stage, (b) aberration compensation obtained by the genetic feedback tuning loop, and (c) phase holograms with compensation at the 553rd generation stage (stagnated state).

ror as -100 , and that of the boundary length as 0 for calibrating the SLM or -0.0132 for the aberration compensation. Since the genetic algorithm is programmed to find the maximum, the cost value is defined as a negative value of the form.

B. Calibration of the Liquid-Crystal Spatial Light Modulator

Here we discuss in detail the calibration of the SLM used in our system. To calibrate the SLM, we obtain the phase-modulation tables of the SLM by two methods. The first is a classical interferometric experiment, and the second is the genetic feedback tuning loop. A comparison between the results for the two methods is also presented in this section.

In this paper a twisted-nematic (TN) LC display (Sony LCX016AL-6 with 8 bit resolution) is used as the SLM. With the SLM control program (Holoeye LC2002), we set the contrast and brightness parameters to 198 and 102, respectively, which are the parameters for adjusting the range and mean value of the voltage impressed on the LC cell. A laser (Coherent DPSS Nd:YAG) with a wavelength of 532 nm is used as the light source, and the diffraction image is captured by a CCD (Kodak MegaPlus ES1.0/MV with 8 bit resolution). The optical transmission power is measured with an optical powermeter (Newport 1835-C). Figure 4 shows a schematic diagram of the interferometer used to measure the phase modulation and the amplitude transmission of the SLM, which is similar to the well-known Mach-Zehnder interferometer. When the SLM is operated in the phase-modulation mode, two linear polarizers are placed before and behind the SLM. The latter polarizer is conventionally referred to as an analyzer. The rotation angle of the polarization is defined as the positive angle between the axis of the polarizer and the director axis of the TN LCSLM at the input face. In our system the rotation angles of the polarizer and analyzer were selected as $\Psi_p = 330^\circ$ and $\Psi_A = 10^\circ$, respectively. The fringes of the interference pattern are captured by the CCD while varying the encoding

indices of the SLM. The phase shift can be calculated from the movement of the fringe, the method for which follows that described in Ref. 15:

$$\text{Phase shift (radiation)} = \frac{2\pi \times \text{Shift of fringe}}{\text{Period of fringe}}. \quad (15)$$

On the other hand, the beam splitter placed behind the analyzer divides the light into two separate arms, and the amplitude transmission (i.e., transmission efficiency) can be measured by using an optical powermeter at the same time as the phase modulation is measured.

The measured phase-modulation and amplitude-transmission tables are plotted in Fig. 5. It can be seen that the phase modulation and amplitude transmission are nonlinear according to the encoding index. The results obtained satisfy the general properties of a TN LCSLM. Phase modulation increases monotonically from 0 to 2π . It increases relatively rapidly around the 190th encoding index, where the amplitude transmission is at a minimum. Generally, in the system using a TN LCSLM with a combination of two linear polarizers, when the phase of an incident optical wave is modulated, the transmission of the wave also changes, since amplitude transmission is somewhat sensitive to polarizer settings. In this paper, because the phase modulation of the SLM is our main concern, the angles of the polarizer and analyzer were set so that the phase modulation would cover the full range from 0 (rad) to 2π (rad). However, it should be noted that our setting of the SLM and polarizers is not sufficient to attain a constant amplitude transmission and that the measured amplitude-transmission characteristic is a nonflat curve as shown in Fig. 5(b).

Next, using the implemented beam-shaping system with the genetic feedback tuning loop, we inspect SLM calibration. The experimental setup is shown in Fig. 2. The circular aperture with a 400 pixel diameter is defined, and the phase hologram calculated with the IFTA is encoded on the aperture area on the

Table 2. Results of Aberration Compensation: Coefficients of the Zernike-Polynomials

Coefficients	Values
A_{00}	0.241605
A_{02}	-0.170412
A_{04}	0.249949
A_{11}	-0.215106
A_{13}	-0.205430
A_{22}	-0.059679
A_{24}	0.237322
A_{33}	0.230890
A_{11}'	-0.245197
A_{13}'	0.245686
A_{22}'	0.248907
A_{24}'	-0.079823
A_{33}'	-0.044566

Table 3. Results of Aberration Compensation: Center Position of Zernike Polynomials

Center Position	Values
x_c	0.999728
y_c	-0.048932

SLM. The target image is a 400×400 pixel image with a T-shaped signal region.

In this experiment an initial population with five chromosomes, $P_0 = \{x_i | i = 1, 2 \dots 5\}$, is created, and the individual chromosome is given as

$$x_i = \left\{ p_{i,n} = \frac{n}{255} \times 2\pi \mid n = 1, 2 \dots, 254 \right\}. \quad (16)$$

The initial population has the same five chromosomes representing the linear phase-modulation table according to the encoding index. The mutation operator is given by

$$x_i' = \begin{cases} p_{i,n} + \Delta(t, 2\pi - p_{i,n}) & \text{for } r_{\text{binary}} = 0 \\ p_{i,n} - \Delta(t, p_{i,n} - 0) & \text{for } r_{\text{binary}} = 1 \end{cases}, \quad (17a)$$

where $\Delta(t, y)$ is defined as

$$\Delta(t, y) = y \left[1 - r^{(1-t/T)^b} \right], \quad (17b)$$

where r_{binary} is a randomly generated binary number, r is a randomly generated real number within $(0, 1)$, t is the ordinal number of the present generation, and T is the ordinal number of the final generation in the genetic algorithm. As seen in Eqs. (17a) and (17b), the upper and lower limits of the variables are 2π and 0 , respectively. The mutation probability is set to 0.03 , and the mutation parameter b , determining the degree of nonuniformity, is tuned to 20 (see Chaps. 5 and 6 of Ref. 10).

The evolution stagnates at the 299th generation, although the maximum number of generations is 1000 . The phase-modulation tables obtained at three different generation stages, the 1st, 43rd, and 299th, are compared in Fig. 6. The phase-modulation curve proceeds to concave downward forms, but the evolution stagnates at a state where the phase-modulation table obtained by the genetic feedback tuning loop does not coincide with that obtained in the interferometric experiment, since the SLM in our system has nonflat amplitude-transmission characteristics. The diffraction image generated by the hologram encoded according to the phase-modulation table of the SLM obtained in the interferometric experiment has a lower cost value than that obtained by the genetic feedback tuning loop. Figures 7(a) and 7(b) show the diffraction image observed at the 1st generation stage and that at the 299th generation stage (the stagnated state). The mean-square errors of these two cases are determined to be 0.3806 and 0.2408 , respectively. This indicates that the latter stage has a higher transmission efficiency than the former, and the average intensities in the signal region also reflect this fact. On the other hand, the normalized variation increases from 0.5742 to 1.198 . However, since the weight of the mean-square error is set 100 times larger than that of the normalized variation, the cost value is consequently improved from -38.23 to

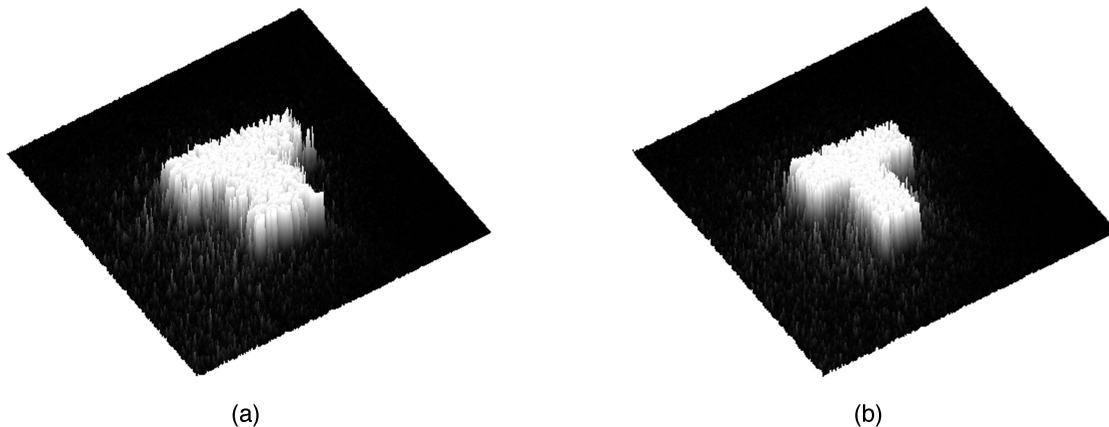


Fig. 9. Diffraction images observed during compensating for aberration with the genetic feedback tuning loop: (a) at the 1st generation stage and (b) at the 553rd generation stage (the stagnated state).

Table 4. Evaluation Parameters of Diffraction Images in Aberration Compensation

Generation	1st Generation	553rd Generation
\overline{GL}_N	195.4	221.8
\overline{GL}_S	22.0	22.5
Mean-square error	0.1494	0.0690
Normalized variation	3.598	1.720
Boundary length	13,130	10,645
Stabilization factor	0.9932	0.9545
Cost value	-191.5	-148.6

-25.41. Detailed data are summarized in Table 1. A significant improvement can be seen by the genetic feedback tuning loop not only in transmission efficiency but also in uniformity.

C. Complementation of the Phase Hologram to Compensate for Aberration

$$x_i = \left\{ p_{l=1 \dots 8} = \frac{A_{nm}}{2\pi} = 0, p_{l=9 \dots 13} = \frac{A_{nm}'}{2\pi} = 0, p_{14} = x_c = 0, p_{15} = y_c = 0 \mid n = 0, 1, 2, 3, m = 0, 1, 2, 3, 4 \right\}. \quad (18)$$

Here we show that the genetic feedback tuning loop is effective in compensating for the aberration of the optics in the digital holographic beam-shaping system. On the hologram plane, the wavefront of the beam is spatially divided by the pixel size of the SLM, and the limit for the aberration compensation in the system is determined by the pixel size and the number of pixels. Since the phase-modulation

table of the SLM has the intrinsic characteristic on a pixel-size scale, finding the optimum phase-modulation table is independent of compensating for the aberration. Therefore the phase-modulation table obtained in Subsection 4.B can be used to encode the hologram on the SLM. As shown in Eq. (7), the coefficients A_{nm} and A_{nm}' and the center position (x_c, y_c) of the Zernike polynomials are unknown variables. Floating-point coding is adopted in the genetic algorithm. The order (m, n) of the circular Zernike polynomial is limited in the interval $0 \leq n \leq 3$ and $0 \leq m \leq 4$. In practice, 15 variables are to be optimized: 8 A_{nm} 's, indicating the coefficients of terms with an x -axis symmetry; 5 A_{nm}' 's, indicating those with a y -axis symmetry; and 2 unknown variables in the center position (x_c, y_c) .

In this experiment an initial population with five chromosomes, $P_0 = \{x_i \mid i = 1, 2, \dots, 5\}$, is created, and the individual chromosome is given as

The initial population has the same five chromosomes, representing a constant phase that leads to no aberration compensation. For encoding the Zernike polynomials on an appropriate scale, the dimension of the SLM plane is scaled so that the diameter of the phase hologram (400 pixels) is set to a unit length and the center of the circular aperture of the encoded phase hologram indicates the position of the coordi-

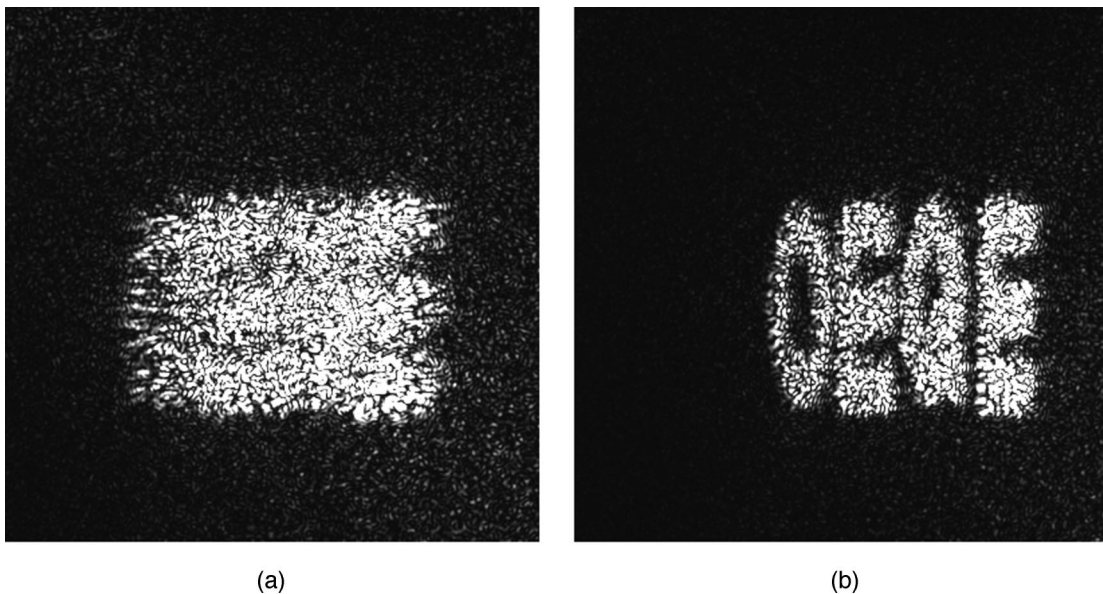


Fig. 10. Diffraction images in the tuned system from holograms (a) without and (b) with aberration compensation, which was previously obtained by the genetic feedback tuning loop.

nate $(0, 0)$. The coefficients of the Zernike polynomials are limited within the range from -0.25 to 0.25 . Therefore the mutation is given by

$$x_i' = \begin{cases} p_{i,l} + \Delta(t, 0.25 - p_{i,l}) & \text{for } r_{\text{binary}} = 0 \\ p_{i,l} - \Delta(t, p_{i,l} + 0.25) & \text{for } r_{\text{binary}} = 1 \end{cases} \quad (19)$$

where $\Delta(t, y)$ holds the same form as shown in Eq. (17b). Here the mutation probability is set to 0.025 , and the mutation parameter b is set to 20 .

In the aberration-compensating experiment, to prove the effectiveness of the genetic feedback tuning loop on aberration compensation, we tilted the CCD at an angle of 10° and tilted the Fourier lens at an angle of -10° , which would effectively induce the internal aberration in the beam-shaping system.

The evolution is stagnated at the 553rd generation, although the maximum number of generations is 1000 . Figure 8 shows how the phase hologram is compensated by the genetic feedback tuning loop. Figure 8(a) shows the phase hologram encoded on the SLM, which is designed without aberration compensation at the 1st generation stage, and Fig. 8(b) shows the aberration compensation obtained from the Zernike polynomials by the genetic feedback tuning loop at the 553rd generation stage. Tables 2 and 3 present the coefficients and center position of the Zernike polynomials at the 553rd generation stage (the stagnated state). Figure 8(c) is the aberration-compensated phase hologram, which is the overlapped image of Figs. 8(a) and 8(b). Figures 9(a) and 9(b) show the diffraction image observed at the 1st generation stage and that at the 553rd generation stage. The boundary length decreases from $13,130$ to $10,645$. The mean-square error and the normalized variation also decrease, and the cost value is consequently improved from -191.5 to -148.6 . Detailed data are summarized in Table 4. As can be seen, the shape of the letter T becomes clearer after aberration compensation.

To verify the effect of tuning the system with aberration compensation, another phase hologram designed with the IFTA algorithm, which regards a system free from the aberration, is encoded on the SLM. Figure 10(a) shows the diffraction image, which is distorted owing to aberration, which was not considered in the IFTA algorithm. Figure 10(b) shows the diffraction image for the phase data with aberration compensation by adopting the compensation profile of Fig. 8(b). Although the letters cannot be identified in Fig. 10(a), the letters OEQE can be read clearly in Fig. 10(b). As seen in the results, the proposed genetic feedback tuning loop is effective for the aberration compensation of a digital holographic beam-shaping system with a SLM.

5. Conclusion

In conclusion, the findings herein show that the proposed genetic feedback tuning loop can be used suc-

cessfully to properly calibrate the LCSLM of a real-time digital holographic beam-shaping system and to encode the aberration-compensated phase holograms, thus overcoming the aberration of the internal optics of the system. The genetic feedback tuning loop is an adaptive, system-independent, and automatic mechanism for tuning the general digital holographic beam-shaping system. It is expected that the proposed technique would be useful in refining more complex digital holographic beam-shaping systems than those dealt with in this paper.

References

1. J. Tarunen and F. Wyrowski, *Diffraction Optics for Industrial and Commercial Applications* (Wiley, 1997).
2. B. Kress and P. Meyrueis, *Digital Diffraction Optics: An Introduction to Planar Diffraction Optics and Related Technology* (Wiley, 2000).
3. V. A. Soifer, V. V. Kotlyar, and L. Doskolovich, *Iterative Methods for Diffraction Optical Elements Computation* (Taylor & Francis, 1997).
4. K. Choi and B. Lee, "A single-stage reconfigurable 2-D optical perfect-shuffle network system using multiplexed phase holograms," *IEEE Photon. Technol. Lett.* **17**, 687–689 (2005).
5. K. Choi, H. Kim, and B. Lee, "Full-color autostereoscopic 3D display system using color-dispersion-compensated synthetic phase holograms," *Opt. Express* **12**, 5229–5236 (2004).
6. K. Choi, H. Kim, and B. Lee, "Synthetic phase holograms for auto-stereoscopic image display using a modified IFTA," *Opt. Express* **12**, 2454–2462 (2004).
7. H. Kim and B. Lee, "Optimal nonmonotonic convergence of the iterative Fourier-transform algorithm," *Opt. Lett.* **30**, 296–298 (2005).
8. H. Kim, B. Yang, and B. Lee, "Iterative Fourier transform algorithm with regularization for the optimal design of diffractive optical elements," *J. Opt. Soc. Am. A* **12**, 2353–2365 (2004).
9. L. Hu, L. Xuan, Y. Liu, Z. Cao, D. Li, and Q. Mu, "Phase-only liquid-crystal spatial light modulator for wave-front correction with high precision," *Opt. Express* **12**, 6403–6409 (2004).
10. Z. Michalewicz, *Genetic Algorithms + Data Structures = Evolution Programs* (Springer-Verlag, 1999).
11. H. Kim and B. Lee, "Calculation of the transmittance function of a multilevel diffractive optical element considering multiple internal reflections," *Opt. Eng.* **43**, 2671–2682 (2004).
12. H. Kim and Y. H. Lee, "Unique measurement of the parameters of a twisted-nematic liquid-crystal display," *Appl. Opt.* **44**, 1642–1648 (2005).
13. J. Reményi, P. Várhegyi, L. Domjan, P. Koppa, and E. Lorincz, "Amplitude, phase, and hybrid ternary modulation modes of a twisted-nematic liquid-crystal display at ~ 400 nm," *Appl. Opt.* **42**, 3428–3434 (2003).
14. J. Nicolás, J. Campos, and M. J. Yzuel, "Phase and amplitude modulation of elliptic polarization states by nonabsorbing anisotropic elements: application to liquid-crystal devices," *J. Opt. Soc. Am. A* **19**, 1013–1020 (2002).
15. M. C. Gardner, R. E. Kilpatrick, S. E. Day, R. E. Renton, and D. R. Selviah, "Experimental verification of a computer model for optimizing a liquid crystal display for spatial phase modulation," *J. Opt. A* **1**, 299–303 (1999).
16. M. Born and E. Wolf, *Principles of Optics*, 7th ed. (Cambridge U. Press, 1999).